Towards solar metallurgy: iron ore reduction by ammonia under concentrated light flux

Marion Luu, Bastien Sanglard, Sébastien Lachaize, Julian Carrey

Towards solar metallurgy: iron ore reduction by ammonia under concentrated light flux

Marion Luu*, Bastien Sanglard*, Sébastien Lachaize, Julian Carrey

Laboratoire de Physique et Chimie des Nano-Objets (LPCNO), Université de Toulouse, INSA, CNRS UMR 5215, UPS, 135 av. de Rangueil, 31077 Toulouse Cedex 4

* : these authors contributed equally to the work.

Key-words: Concentrated solar power; Ammonia; Hydrogen; Iron oxide; Metallurgy; Sustainability

Abstract:

Iron and steel making are responsible for around 7% of global CO_2 emissions. The use of fossil fuels to provide both the heat needed to reduce iron ore into iron and the reducing agent is the principal cause of these emissions. Here, we focus on an alternative pathway for direct iron ore reduction using concentrated light power as the heat source and ammonia as the reducing gas. Experiments were performed on industrial iron ore pellets and compared to the ones obtained using hydrogen as a reducer. We showed that below 600°C, reduction with ammonia proceeds via iron nitrides formation. Reduction dynamics is slower for ammonia for short exposure times but is rapidly caught up, so that reduction ratios as high as the ones obtained for hydrogen are observed. Notably, degrees of reduction exceeding 90% in 5 min were obtained on disks cut from industrial iron ore pellets. This work therefore opens a promising route towards ammonia-based solar metallurgy.

I. Introduction

Iron and steelmaking are a cornerstone of our current society - 1951 Mt of steel were produced in 2021 [1] - but are responsible for around 7% of global CO_2 emissions [2]. Whatever the route used to produce steel, fossil fuels are used to chemically reduce the iron ore and/or to provide the heat needed. Strongly decarbonizing the ironmaking process is a necessary endeavour that requires using carbon free or bio-sourced reducers and a less emitting heat source. In the present work, we aim at studying the direct reduction of iron oxides via the combined use of ammonia as the reducer and concentrated solar power as the heat source, for reasons which are detailed below.

Concerning the use of carbon-free reducers, the direct reduction of iron oxide (Fe_2O_3) by hydrogen (H_2) is promising and is described by the following equation:

$$Fe_2O_3 + 3\,H_2 \rightarrow 2\,Fe + 3\,H_2O \qquad \mathbf{1}$$

In this reduction, two intermediary iron oxides can be formed depending on temperature: magnetite (Fe_3O_4) and wuestite (FeO). This route has largely been studied in the literature [3–8] and is currently developed by several companies [9,10].

However, transporting H_2 under its compressed or liquid form from places of production to places of use presents some drawbacks, such as the energy cost and the lack of dedicated infrastructures.

Ammonia (NH_3) might be an advantageous alternative. Although producing NH_3 from H_2 requires an additional synthesis step, ammonia is liquefied at lower pressures and higher temperatures than hydrogen, making it a high-density hydrogen carrier (108 kg H_2/m^3 liquid NH_3) suitable for transportation. Its advantages are also already existing transport facilities, storage infrastructures and workers [11]. Finally, it can be efficiently decomposed into hydrogen for further use (Equation 2), several catalysts being active for this purpose [12]. These benefits explain why ammonia is seriously considered as an energy carrier in off-shore wind farms, for example [13,14].

$$2\ NH_3 \rightarrow 3\ H_2 + N_2 \qquad 2$$

Besides the reduction of iron ore by hydrogen after ammonia decomposition, the direct reduction by ammonia is also possible [15–20]. Injecting NH_3 into the reactor makes also sense since iron and iron alloys are known catalysts of NH_3 decomposition [11]. Hosokai *et al.* showed that from 430 °C to 530 °C, a direct reduction via ammonia occurs (Equation **3**) and that over 530 °C, the mechanism is an indirect reduction via the hydrogen produced by NH_3 thermal decomposition [15].

$$Fe_2O_3 + 2\ NH_3 \rightarrow 2\ Fe + N_2 + 3\ H_2O \qquad \mathbf{3}$$

Their experiments were conducted under low concentrated ammonia flux and they observed the formation of iron nitride Fe_4N. Yasuda *et al.* showed that, with higher concentrations of ammonia, the iron produced in presence of NH_3 is nitrided into a $Fe_{3-x}N$ phase ($0 \leq x \leq 1$), which gradually decomposed into Fe_4N and finally iron [16] (see Equation **S.I.11** in the **Supplementary Information**). All in all, Hosokai and Yasuda proposed the following nitridation pathways:

$$\frac{8}{11}\ Fe_3O_4 + 2\ NH_3 \rightarrow \frac{6}{11}\ Fe_4N + \frac{6}{11}\ H_2 + \frac{8}{11}N_2 + \frac{32}{11}\ H_2O \qquad \mathbf{4}$$

$$y\ Fe + \ NH_3 \leftrightarrow Fe_yN + \frac{3}{2}\ H_2 \qquad \mathbf{5}$$

Ma *et al.* then showed that the nitride phase contained in a sample could be removed during a subsequent melting process to leave only the iron phase [18]. Moreover, they highlighted the fact that nitriding allows the protection of iron against re-oxidation and other degradations. This indicates that nitriding does not have to be seen as a problem and that iron nitrides can potentially be included in the reaction yield.

As for the heat source, concentrated solar power for metallurgy is an option that is being studied since Steinfeld and Kuhn in 1993 [21]. They worked on the reduction of magnetite (Fe_3O_4) by methane under concentrated solar flux and were able to reach 68% of reduced iron for a sample heated for 15 min at 1000 °C. Later, Fernández-González *et al.* studied the reduction of sintered ore with coke breeze and reached 29.7% reduction [22].

The combined used of hydrogen and concentrated solar power for the direct reduction of iron ore has only been studied by Li *et al.* [23], Abanades and Rodat [24] and by our team [25]. Li *et al.* obtained 98% reduction after 50 min on a fine powder in an indirectly heated reactor. Abanades and Rodat were able to completely reduce 1 g of iron oxide particles mixed with sand in 15 min at 1000 °C. In our case, a direct reactor was used, where the samples – industrial ore pellets – were directly heated by the light flux. It was shown that, in a direct reactor, the reaction is fast and propagates from the illuminated side [26]. By playing on the shape of the samples to take this mechanism into account, we were able to reach a reduction yield of 96% in 2 min on flat and thin samples elaborated by slicing industrial hematite ore pellets.

To our knowledge, the use of both ammonia and concentrated light flux has never been studied. The underlying issue is whether it is possible to reach reduction yields as large as the ones obtained

with hydrogen in similar times. To address it, we carried out batch experiments on industrial hematite pellets and thin samples exposed to direct light irradiation under ammonia and compared them to the results obtained with hydrogen. We observed a difference in the reduction kinetics for low exposure times. Nonetheless, we were still able to reach high reduction yields: a value of 95% was obtained after 6 min on 2 mm-thick disk samples.

II. Experimental section

II.1. Materials

The samples were industrial pellets courtesy of ArcelorMittal (Maizières-lès-Metz, France); phase ratios according to XRD analysis are available in **Table S.I.1**. Experiments in an *in situ* XRD chamber (XRD 900, Anton Paar) were conducted with industrial pellets grinded in powder with a mortar and pestle. For the reductions under concentrated light flux, pellets were chosen with a mean weight of 2.13 g (±0.5%). Disks were cut from larger pellets using a diamond circular saw (Buehler IsoMet low speed saw; Buehler – n°114254). Their mean weight, diameter and thickness were 0.75 g, 11.31 mm (±3.5%) and 2.13 mm (±2.4%) respectively.

II.2. *In situ* XRD experiments on powders

In situ XRD experiments of powder reduction were performed using a PANalytical Empyrean diffractometer (45 mA, 35 kV, Co) mounted with the reaction chamber. For all experiments, an atmosphere of NH_3-N_2 at 5-95 vol.% (Air liquid) was used at 1 bar. For each analysis, the temperature was risen to the set-up value at a rate of *ca.* 130 °C/min and then maintained during the plateau. Each plateau was composed of nine successive scans of 20 min each, with one additional scan realised at 30 °C before the rise in temperature. These scans were performed in a Bragg-Brentano scanning geometry from $2\theta = 10°$ to 110° with a 0.0263° step and a counting time of approximately 70 s.

II.3. Reduction under concentrated light flux

The experimental bench was composed of a Xenon lamp (9 mm-long arc, electric power of 1230 W, light power of 300 W_l) placed at the first focal point of an ellipsoidal mirror (XE1600, ScienceTech). A schematic of the set-up can be found in **Figure S.I.1**. An alumina crucible (Sceram ceramics) was placed inside a 0.6 L borosilicate glass reactor (Avitec) and this reactor was placed on a mobile *xy* platform (2 XR25C Travel Linear Translation Stage mounted at 90°, ThorLabs), the *z*-axis displacement being realized with a rack and pinion. The crucible was aligned with the concentrated light flux and the position along the *z*-axis was chosen according to the crucible type. For the pellets, a 16 mm-diameter crucible was used and placed a few centimetres below the second focal point of the mirror to be fully illuminated. For the disks, another 16 mm-diameter crucible was used with a few modifications: it was cut so that two alumina bars could serve as a support for the disks allowing the reducing gas to be in contact with the lower surface of the disk. It was placed so that its top would be at the same place as the top of the other crucible; the disk samples where thus completely illuminated. In both cases, the crucible was receiving around 150 W_l and the mean luminous flux was around 75 W_l/cm^2 (maximum of 115 W_l/cm^2 at the center, see Figure S.I.3). Pictures of the two crucibles are displayed in **Figure S.I.2**.

In standard experiments, temperature was measured with two K-type thermocouples: one placed under the crucible and the other one in the atmosphere, not directly under the light flux. We also performed specific experiments in which the first thermocouple was placed directly under an iron ore pellet, through a hole pierced in the crucible while the second thermocouple was in direct contact

with the top (see Figure S.I.9). These experiments aimed at estimating the temperature gradient within the pellet. The reactor pressure was measured with a pressure sensor (type 520, Huba control). Temperature and pressure were acquired in real-time using a Labview program.

Before each experiment, the reactor was successively vacuumed and refilled three times with the reducing gas before setting it at the required pressure. For hydrogen reductions, hydrogen was produced by water electrolysis using a H_2 generator (F-DGSi, model WM-H2) and the pressure was set at 2.5 bar(g) (*i.e.* 3.5 bar(a)). For ammonia reductions, a bottle of pure NH_3 (H_2O < 100 ppm, AlphaGaz™) was used and the pressure was set at 1.33 bar(g) (*i.e.* 2.33 bar(a)) which corresponds, once fully decomposed into H_2, to the same amount of H_2 than the hydrogen reductions (Equation 2). Some samples were rolled-over so that several sides would be exposed to the light flux. In this case, after the first exposure, the light flux was stopped, the reactor was returned to ambient atmosphere, the sample was rolled-over and the reactor was flushed three times with the reducing gas before setting it at the required pressure.

For some specific experiments, the composition of the reactor atmosphere thorough the reduction was also measured using a quadrupole mass spectrometer (Pfeiffer Omnistar GSD 320). For this purpose, the reactor was connected to the spectrometer by a capillary and a fine stainless steel metering valve (Milli-Mite 1300 Series, Hoke). Before each gas analysis the dead volume between the spectrometer entry and the valve was pumped, the valve being closed. After pumping, the valve was opened and the gas analysed. This protocol allows to analyse the gas inside the reactor every *ca.* 1 min 30 s.

Once reduced, the samples were grinded using a mortar, pestled into a fine powder and analyzed with a PANalytical Empyrean diffractometer (45 mA, 35 kV, Co). For the pellets, about 90% of the grinded sample was placed in a sample holder and one scan per sample was carried out. For the disks, for which less powder was produced, a smaller sample holder was used and two scans per sample were conducted with about 20% of the powder per batch to get a reliable analysis of the sample. These scans were performed with the same parameters as the ones used for *in situ* XRD experiments (see above).

Once reduced by ammonia or hydrogen, some pellets were coated in epoxy and then cut from top to bottom with a diamond circular saw (Buehler IsoMet low speed saw; Buehler – n°114254).

II.4. Characterization

The diffractograms were analysed using the HighScore software to identify the phases in presence. The Crystallographic Information File (CIF) files were obtained via the Crystallography Open Database website and the mass proportion (%) of each phase was determined with MAUD software using Rietveld refinements. For each diffractometer, the weighted reliability factor (R_{wp}) was kept below 10% and the agreement between the experimental values and the fit was visually validated (see **Figure S.I.14** for reference).

To quantify the reduction degree of the samples, two different quantities were used: the degree of metallization (DoM) and the degree of reduction (DoR), both expressed in percent. The first indicates the weight ratio between the metallic iron and the iron contained in all iron-containing phases (Equation **6**). The second is similar but counts in addition the iron contained in nitrides (Equation **7**). For the reductions by hydrogen, DoM and DoR are equal but, in the case of ammonia, introducing the DoR allows to integrate the nitrides into the potentially useful material since the iron contained within them is retrievable once the material is melted [18].

The detail of the DoR and DoM obtained for each experiment can be found in **Table S.I.2**.

$$\mathrm{DoM} = \frac{\text{pure iron (wt.\%)}}{\text{iron contained in all phases (wt.\%)}}\,(\%) \qquad \textbf{6}$$

$$\mathrm{DoR} = \frac{\text{pure iron + iron contained in nitrides (wt.\%)}}{\text{iron contained in all phases (wt.\%)}}\,(\%) \qquad \textbf{7}$$

III. Results and discussion

III.1. Influence of temperature

Figure 1 shows the evolution of the phase proportion for five powder samples exposed to different temperature plateaus in an *in situ* XRD chamber under an ammonia atmosphere: 400 °C, 450 °C, 500 °C, 550 °C and 600 °C. The diffractograms used to determine the phases are available in **Figures S.I.4-S.I.8**.

At 400°C, only the partial transformation of hematite in magnetite is observed (see **Figure 1a**). At 450°C, hematite is transformed into magnetite and a small amount of iron nitride $Fe_{3-x}N$ ($0 \leq x \leq 1$) appears, the rise of the latter being correlated to a decrease of the magnetite content (see **Figure 1b**). Yasuda *et al.* [16] also observed the transformation of magnetite into $Fe_{3-x}N$ at approximately the same temperature. The first apparition of iron is observed for the experiments performed at 500°C, but its part stays below 20%, even after 200 min of reaction (see **Figure 1c**). This temperature also corresponds to the apparition of iron nitride Fe_4N which starts to slowly decompose into iron after 150 min. This decomposition was also observed by Iwamoto *et al.* [17]. At 550 °C, hematite is quickly transformed into magnetite and iron nitrides, which then decompose into iron (see **Figure 1d**). The nitrides are fully converted into iron in less than 60 min. The remaining of the reaction is a slow transformation of magnetite into iron, the later composing 90 wt.% of the sample after 200 min. Finally, at 600 °C (**Figure 1e**), hematite is immediately transformed, the noticeable difference being the apparition of a small amount of wuestite and the fact that no nitrides are detected. The absence of nitrides could be explained either by the quick decomposition of ammonia at this temperature, making hydrogen reduction predominant over nitriding, or by the iron nitride fast decomposition compared to the XRD scan duration. For this temperature plateau, the iron ratio reaches 87 wt.% after 60 min. Afterwards, the small amount of wuestite and magnetite still present in the sample (*ca.* 7 wt.% and 5 wt.% respectively) slowly decomposes into iron, which constitutes 96 wt.% of the powder at the end of the heating plateau. The apparition of wuestite is coherent with a reduction by hydrogen since at temperatures higher than 570 °C, the hydrogen reduction of hematite goes through wuestite formation (see Equation **S.I.6-S.I.8** and Ranzani Da Costa [27]).

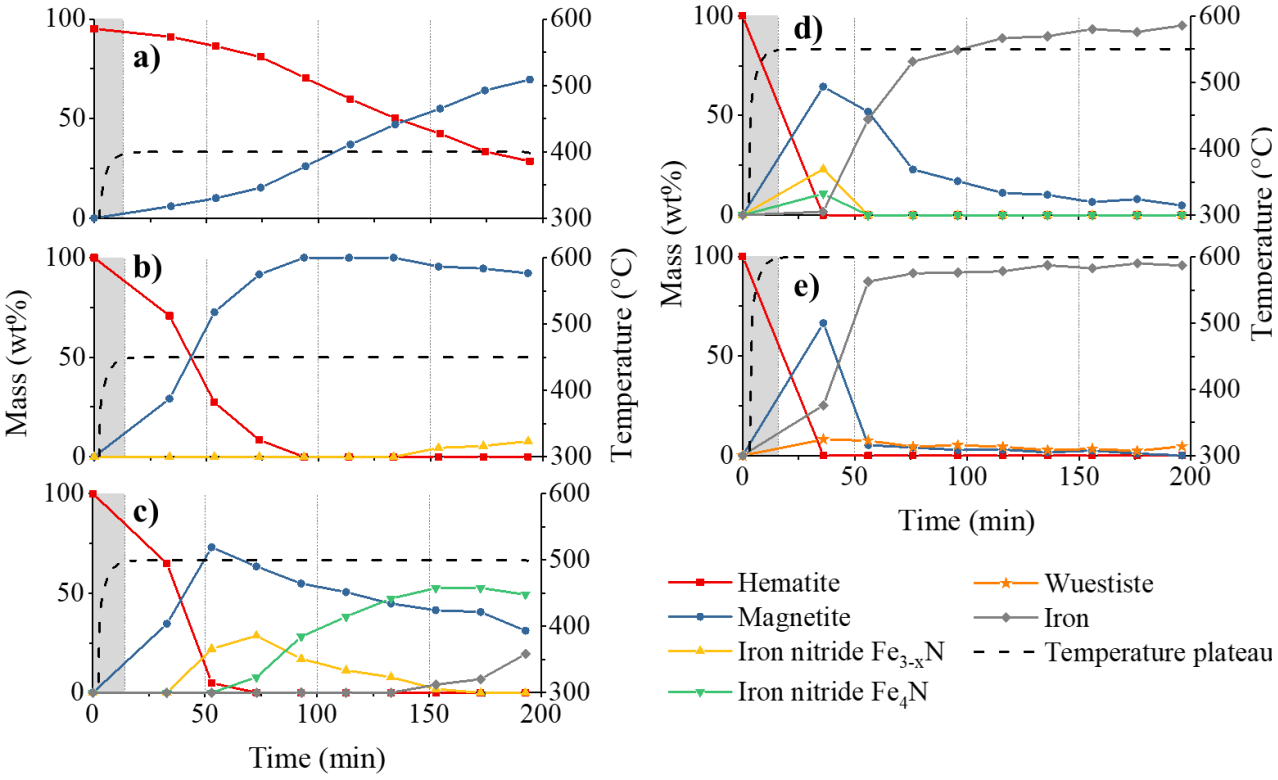

***Figure 1**: Phase evolution as a function of time for different temperatures (a) 400 °C, b) 450 °C, c) 500 °C, d) 550 °C and e) 600 °C). Temperature is in dashed black line and the rising time has been greyed out.*

III.2. Reduction under concentrated light flux

In this section, ammonia and hydrogen reductions of industrial hematite pellets under concentrated light flux were conducted. The aim was here to compare ammonia and hydrogen reduction on the same types of samples and under conditions similar to our previous work [25]. To do so, the ammonia content was chosen so that, if totally decomposed, the hydrogen content would be the same as for the hydrogen reductions. Thus, 3.5 bar(a) of hydrogen (corresponding to a 3.5:1 ratio of hydrogen:reduced iron) and 2.33 bar(a) of ammonia were chosen.

First, specific experiments were performed on pellets, aiming at giving access to the appearance of the reduction front and to the temperature of the pellet during the reaction. The pellets, labelled H2-P28 and NH3-P28, were exposed 28 min to the light flux in a hydrogen and ammonia atmosphere, respectively. The micrographs of the pellets cut in two are shown in **Figure 2**.

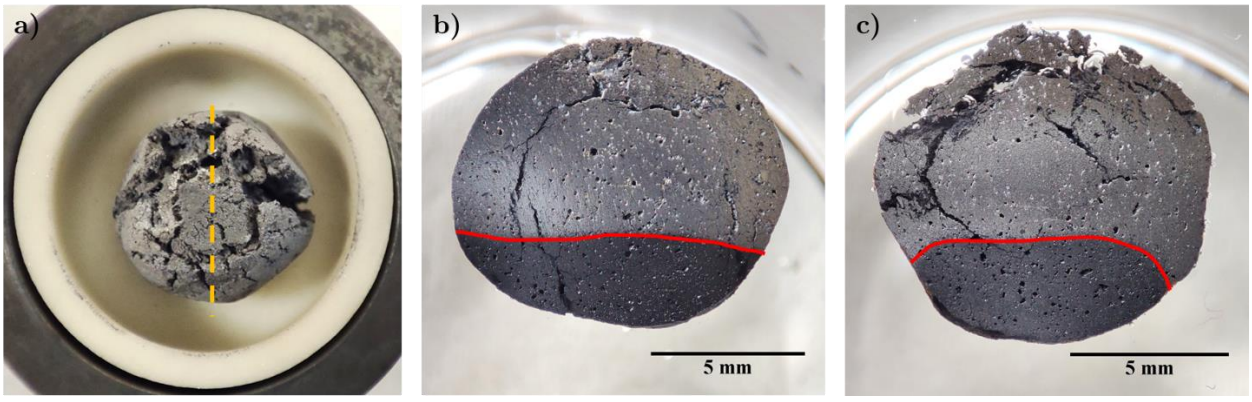

Figure 2: a) Top view of NH3-P28 pellet before cutting. The dashed yellow line corresponds to the cut line. Optical microscopy micrographs of b) H2-P28 and c) NH3-P28 pellets after their cut. The red line corresponds to the reduction front: the material above the line is iron whereas it is iron oxide below the line.

The top and bottom of the sample have very different colours (see **Figure 2**). It was shown in our previous work related to the hydrogen reduction of pellets that light grey is pure iron whereas dark grey is iron oxide, indicating that the reduction proceeds from the illuminated side of the pellet to the shadowed one [25].

Figure S.I.10 shows the results of dedicated experiments on H2-P28 and NH3-P28 where thermocouples were put in contact with the top and the bottom of the pellets. The top-temperature reaches 1000 °C within the first 100 s of the experiment and changes little thereafter. The temperature below reaches 250 °C within the first 250 s, then continues to rise slowly to 300 °C at the end of the reaction. We note a slight difference between the two reducers: reduction under ammonia leads to a higher temperature compared to H_2. The difference for the top temperature peaks at around 90 °C at 4 min before decreasing to around 40 °C after 28 min. A slightly less important difference is observed for the bottom temperature. The range of measured temperatures perfectly agrees with the presence of non-reduced ore at the bottom of the pellet and of iron at the top, since iron starts to be efficiently produced in H_2 and NH_3 reduction experiments for temperatures above 550 °C (see **Figure 1** and [28]). These results have led us to conduct experiments where the pellets were rolled over to expose different sides to the light flux, in order to decrease the total reduction time (see below).

To continue the study, for each gas, three additional experiments were conducted: two on pellets exposed for different times and one on a disk exposed for 2 min. The pellets, labelled H2-P16, H2-P12, NH3-P16 and NH3-P12, were rolled-over so that different sides would be exposed to the light flux. For ammonia reduction, other disks were reduced for longer exposure times. **Table 1** summarizes the experimental conditions.

***Table 1**: Overview of the hematite samples. The sample reference provides indication on the gas used for the reduction (NH_3 or H_2), the type of sample (D for disk; P for pellet) and the total reaction time. For the rolled-over samples, the total exposure time is the number of exposed sides times the duration of each exposure. All the reductions were conducted with a maximum light flux of 115 W_l/cm^2. The pellets weight ca. 2.13 g and the disk samples 0.75 g with a diameter of ca. 11.31 mm and a thickness of ca. 2.13 mm.*

Reducing gas	Sample	Sample description	Exposure time (min)
3.5 bar(a) H_2	H2-P28	Pellet	28
	H2-P16		16 (2 × 8 min)
	H2-P12		12 (4 × 3 min)
	H2-D2	Disk	2
2.33 bar(a) NH_3	NH3-P28	Pellet	28
	NH3-P16		16 (2 × 8 min)
	NH3-P12		12 (4 × 3 min)
	NH3-D2	Disk	2

	NH3-D3		3
	NH3-D4		4
	NH3-D5		5
	NH3-D6		6
	NH3-D7		7
	NH3-D8		8

III.2.a. Comparison with hydrogen-based reduction for different samples

The first four samples for each reducing gas are compared in this section. The diffractograms used to determine the phases and the DoR and DoM values are available in **Figure S.I.12** and **Table S.I.2**.

Figure 3 shows the DoR and the DoM after their reduction by hydrogen (in green) or ammonia (in shades of red). In the case of the pellets exposed for 28 min and not rolled-over (H2-P28 and NH3-P28), the DoR reached with hydrogen is slightly higher than with ammonia and one can note that no nitrides were observed at the end: the DoR and DoM for ammonia reduction are the same. They start to differ for a pellet exposed 16 min with a rollover after 8 min; in this case, a small amount of nitrides is produced resulting in a DoR of 98.1% and a DoM of 97.0% (NH3-P16) against 95.9% for hydrogen reduction (H2-P16). The DoR reaches 96.2% for the hydrogen reduction of a pellet exposed 4 × 3min (H2-P12) but only 77.1% for the ammonia reduction of a similar pellet (NH3-P12); the DoM is even lower (45.8%). For the disks exposed for 2 min (H2-D2 and NH3-D2), the DoR is 95.6% with hydrogen while only 57.5% with ammonia, the DoM being only 39.7%.

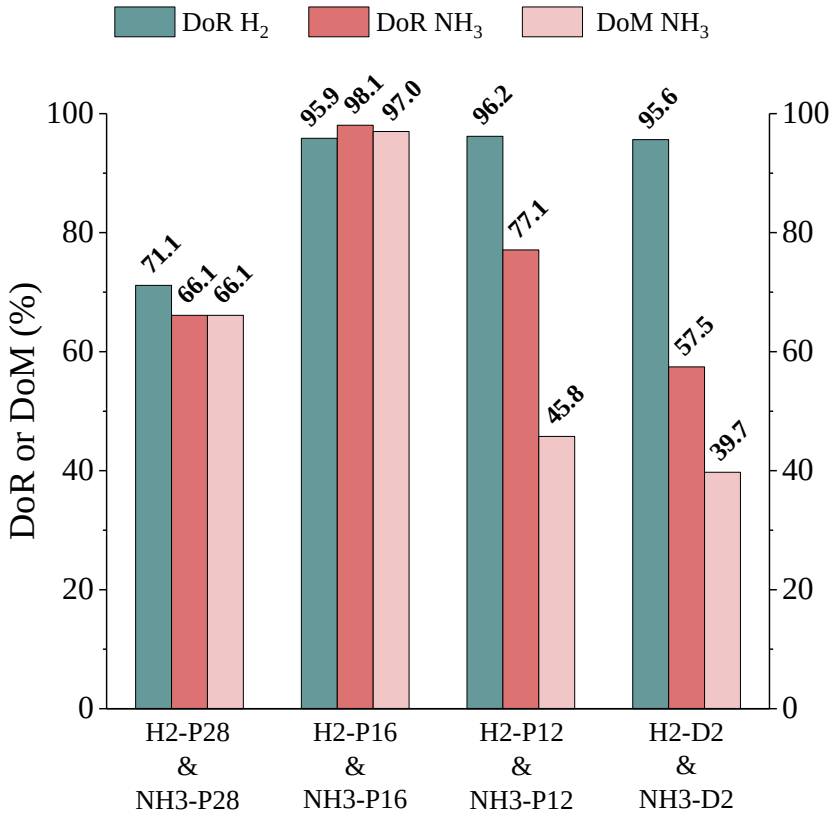

***Figure 3**: Degree of reduction (DoR) or degree of metallization (DoM) of different samples reduced by H_2 (green) or NH_3 (red). For NH_3 the DoR and DoM are different and are represented*

in dark and light red respectively. The samples are, from left to right, pellets exposed for 28 min to the light flux, pellets exposed for 16 min with one rolling-over, pellets exposed for 12 min with three rolling-over and disks exposed for 2 min.

We were here able to observe the same behaviour as our previous work as the hydrogen DoR is greater than 90% for pellets rolled-over, a value higher than for a longer exposure time without rollover. The DoR for the disks reduced under hydrogen was also higher than 90% due to its thin shape.

The behaviour observed with ammonia is different: the DoR was lower than with hydrogen, except for the 16 min exposure. For a pellet exposed 12 min, each side was exposed for only 3 min and in this case, a difference of around 20% between ammonia and hydrogen reductions was observed. For the disk exposed 2 min, a little less than 40% of difference can be noted. This indicates that under these conditions, the global ammonia reduction kinetics is slower than the one with hydrogen, at least when we proceed by short exposures in a row. This slower reduction by ammonia than by hydrogen was also observed by Yasuda et al [16] even though they were working with an infrared furnace. This could be explained by the much larger size of ammonia molecules compared to hydrogen, making more difficult their diffusion inside the samples (0.310 nm against 0.074 nm of molecular diameter for ammonia and hydrogen respectively). Indeed, for temperatures lower than 530 °C, NH_3 is the only reducing gas but when higher temperatures are reached, H_2 is produced and interferes in the reduction [15]. Therefore, at short exposure times, we suggest that the NH_3/H_2 ratio stays in favour of NH_3, *i.e.* that the reduction happens in a slower diffusion regime than with pure H_2. This hypothesis is confirmed by the NH_3/H_2 ratio measurements made during a specific experiment on NH3-P28: it does not drop below 1 before 4 min (see **Figure S.I.11**). Otherwise, the slower kinetics could also be due to a higher activation energy for ammonia than for hydrogen, but no data for ammonia permitting to evaluate this hypothesis were found in the literature.

Another difference with pure hydrogen reduction is the production of nitrides: iron nitrides are present as $Fe_{3-x}N$ in the disk exposed 2 min and as Fe_4N in the pellet exposed 4 × 3 min (see Figure S.I.12). It can be observed that there are no iron nitrides left after long and continuous exposure times (DoR and DoM are equal). We attribute it to the fact that iron nitrides decompose at high temperatures, as previously observed in the literature and in **Figure 1**. The mechanisms of nitridation for the samples exposed several times for short durations can be complex and will thus be discussed in details in **Section III.3**.

III.2.b. Optimization of the degree of reduction for disks samples

Figure 4 shows the DoR and the DoM of disk samples exposed to the concentrated light flux for different durations. Diffractograms are available in **Figure S.I.13** and DoR and DoM values can be found in **Table S.I.2**. A sharp rise is observed for low exposure times (below 5 min) for both DoM and DoR. Then the curves reach a plateau with a DoM and DoR greater than 95% after 6 min.

This further shows the globally slower kinetics of ammonia reduction for short exposure under the concentrated light flux and confirms the production of nitrides and their disappearance for longer reductions. Diffractogram analysis from Figure S.I.13 reveals the presence of a mixture of $Fe_{3-x}N$ and Fe_4N after 2 min of exposition, while only Fe_4N is present after 3 min and 4 min. Iron nitrides are finally totally decomposed after 5 min.

These experiments show that it is possible to considerably reduce the reaction time with a thin sample. Indeed, only 5 min are necessary to get a DoM greater than 90%, which makes this process approximately three times faster than the best ones with pellets (see **Figure 3**, NH3-P16). We attribute it to a homogenous and higher temperature than for pellets. This implies that iron can be quantitatively produced and nitrides fully decomposed for lower reaction times.

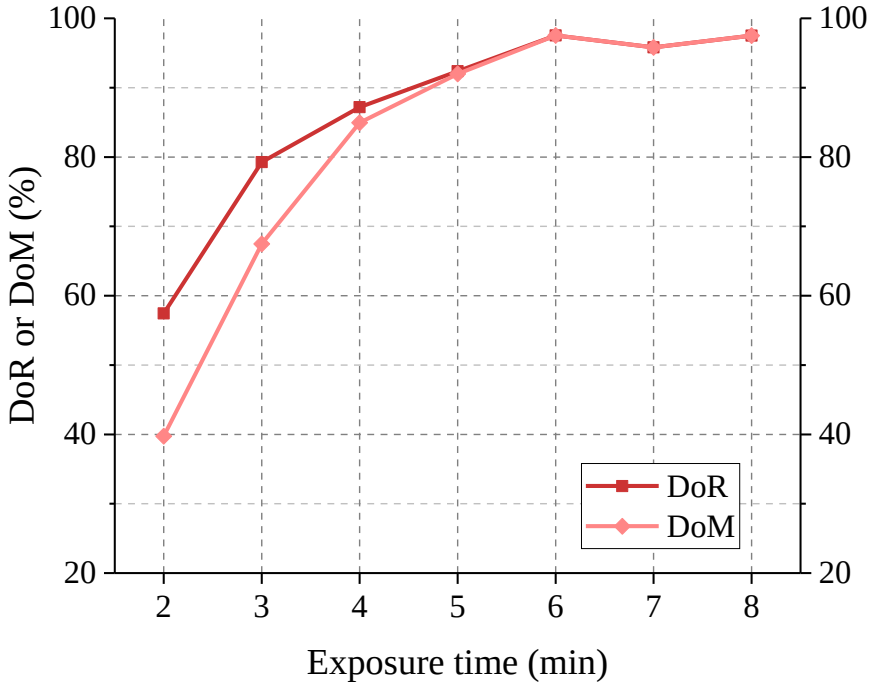

***Figure 4**: Degree of reduction (DoR) and degree of metallization (DoM) of hematite disks samples exposed to the luminous flux for different time durations.*

III.3. Discussion

In this section, the temperatures measured during some pellet experiments, the nitriding mechanism as well as the potential industrialisation of a solar and ammonia-based metallurgy process will be discussed.

First, as shown in **Figure S.I.10**, the temperatures reached during ammonia reduction are higher than the ones reached during hydrogen reduction. One can note that the difference peaks at 4 min. This could be due to the fact that ammonia reduction is slower and less endothermic than hydrogen reduction [15]. However, we still observe a difference after 28 min which can hardly be explained by this reason since ammonia is completely decomposed. This difference could be explained by the final atmosphere composition: the presence of a heavier gas, nitrogen, could change the thermal exchanges between the pellet, the luminous flux and the thermocouple.

In the literature, nitriding has been observed during the reduction as well as during samples' cooling in the presence of ammonia [18,20]. Our experiments on powders confirmed the nitriding during reduction (see **Figure 1**) but our experiments on pellets are more delicate to interpret (see **Figure 3** and **Figure 4**). Indeed, for long exposure times (28 min and 8 min), we observed no nitriding but it could be attributed to the decomposition of nitrides produced during the reduction as well as to the absence of ammonia in the cooling atmosphere (see the NH_3/H_2 ratio in **Figure S.I.11**).

For short exposure times (3 min), there are nitrides in the samples but the conditions are favourable to the production of nitrides during the reduction as well as during the cooling. Indeed, the exposure time could be too short for the nitrides to be decomposed during the reduction and ammonia is still present in the cooling atmosphere: the two processes could therefore be happening. To better illustrate this point, one can take the example of the pellet exposed 4 × 3 min. After a first exposition, the pellet is turned so that its top is mainly oxide and the bottom mainly iron. The atmosphere is filled with ammonia and the pellet illuminated. At the top, the oxide is therefore reduced; the produced iron could then be nitrided by the remaining ammonia during cooling (probably not during the reduction as the temperature is high enough – 1000°C, see **Figure S.I.10** – to directly decompose the nitrides). On the contrary, at the bottom, the already reduced iron part is colder and nitriding without decomposition could occur. At this stage, we are thus not able to determine which process is responsible for the nitriding observed for short exposure times. Further experiments are envisaged to try to solve this issue.

As for the industrial potential of an ammonia-based solar metallurgy, besides the proof-of-concept presented in this paper, further investigation should focus on the design of the reactor. One could for example consider a rotary kiln or rotating cylindric reactor working with iron ore pellets. However, it has been shown here that thin samples are more adapted to short residence times. An efficient reactor should therefore take this constraint into account, and one could imagine the use of thin plates of iron oxide sliding through the light flux. These perspectives were discussed in our previous work and could be considered for ammonia in the same way as for hydrogen [25]. The main difference would be the residence time of the charge since ammonia reduction is kinetically slower at low temperatures and becomes competitive with hydrogen reduction only when a high temperature is reached in the whole sample.

Another necessary study to estimate the industrial potential of solar ammonia metallurgy would be the life cycle assessment (LCA) of ammonia metallurgy compared to the one of hydrogen. Such a study should consider the two possible ways to use ammonia in a metallurgy process: the *in-situ* use of ammonia – as in the present work – or the *ex-situ* one, with a first step consisting of ammonia decomposition into hydrogen. This last possibility could lead to the absence of nitrides in the produced iron and would prevent the kinetics slowdowns observed during ammonia reduction. These considerations on the reducer use will be part of a solar metallurgy LCA that is currently performed by collaborators and that will take into account technical parameters such as the size of the production units, their repartition on a territory, the materials used for construction and, of course, the entire iron ore and reducer supply chains.

To go further on issues related to reducers, one could wonder about their availability for a future low-carbon iron production. Several research groups have estimated the electricity amount required to produce H_2 or NH_3 with low-carbon processes. For hydrogen and for ammonia, around 19.5% and 24.5% of the global electricity production in 2021, respectively, should be assigned to the production of these reducers in order to meet the steel demand of the same year (details on the calculations are presented part G of **Supplementary Information**). Needless to say, if this electricity aims at decarbonizing metallurgy, it should be low-carbon. Such a huge quantity of low-carbon electricity could hardly be available, which logically leads to recall the importance of sufficiency and of redefining our needs facing ecological emergency. In term of iron production, more than half the world steel consumption is used by the building and infrastructure sector [30]. This part alone can be optimized by many options such as a better recycling or reuse [31–33]. Furthermore, other means of construction are explored and could provide a solution to this overuse of steel [34–36]. However, rethinking of needs and uses should be among our priorities.

IV. Conclusion

In the present article, ammonia reduction of industrial hematite samples under concentrated light flux was compared to hydrogen reduction.

First, for powder samples studied by *in situ* XRD, observations from the literature were confirmed, such as the production of iron for temperatures over 500 °C and the production of nitrides that subsequently decompose into iron. The possibility to produce iron at such a low temperature is of great importance when envisaging production units based on solar irradiation. Besides, even if nitrides are produced, they will decompose once the iron produced is melted to the desired shape.

For pellet samples, experiments showed that rolling the samples over was not as much efficient for ammonia reduction than for hydrogen: if the time during which each side is exposed is too short, the degree of reduction is much lower for ammonia than for hydrogen, given that the reaction with ammonia is slower than with hydrogen. However, letting the pellets 2x8 min under the concentrated light flux under ammonia allows to get a DoR of 98.1%, slightly above the DoR reached in 4x3 min under hydrogen.

Finally, disk samples were studied because they can quickly reach a high and homogeneous temperature. For a 2 min exposure, the reduction was less efficient with ammonia than with hydrogen, confirming that short exposure times are not suited for ammonia reduction. However, only 6 min were necessary to reach a plateau above 95% for both the degree of reduction and the degree of metallisation, proving the potential interest of iron reduction by ammonia under a concentrated light flux.

In this work, synthetized ammonia was used but using bio-sourced ammonia could be a way to further reduce the environmental impact of the ironmaking process. Our short term perspective is to use urea, a molecule found in mammals urine, which decomposes into ammonia at temperatures higher than 150 °C [37,38]. Therefore, an iron making process based on concentrated solar power as heat source and bio-sourced ammonia produced by urea decomposition as reducing agent could be considered as a low-emission alternative for ironmaking.

V. Data availability

The data that support the findings of this study are available on request from the corresponding author, S. Lachaize.

VI. Acknowledgements

The authors thank Simon Cayez and Nicolas Ratel-Ramond for XRD and MAUD training as well as Geraldine Ballon, Francis Chouzenoux and Touati Douar for mechanical and technical support. The authors also thank Jose Barros (ArcelorMittal) for the supply of iron oxide pellets. This study and the funding of Marion Luu's PhD have been supported by the Agence Nationale de la Recherche (contract ANR-20-CE05-0008-03, METASOL). Bastien Sanglard's PhD has been funded by INSA Toulouse.

VII. References

[1] *World Steel in Figures 2022*, https://worldsteel.org/steel-topics/statistics/world-steel-in-figures-2022/.

[2] *Iron and Steel – Analysis*, https://www.iea.org/reports/iron-and-steel.

[3] A. Heidari, N. Niknahad, M. Iljana, and T. Fabritius, A Review on the Kinetics of Iron Ore Reduction by Hydrogen, Materials **14**, (2021).

[4] F. Patisson and O. Mirgaux, Hydrogen Ironmaking: How It Works, Metals **10**, 922 (2020).

[5] V. Vogl, M. Åhman, and L. J. Nilsson, Assessment of hydrogen direct reduction for fossil-free steelmaking, J. Clean. Prod. **203**, 736 (2018).

[6] R. R. Wang, Y. Q. Zhao, A. Babich, D. Senk, and X. Y. Fan, Hydrogen direct reduction (H-DR) in steel industry—An overview of challenges and opportunities, J. Clean. Prod. **329**, 129797 (2021).

[7] D. Wagner, O. Devisme, F. Patisson, and D. Ablitzer, A laboratory study of the reduction of iron oxides by hydrogen, (2008).

[8] M. E. Choi and H. Y. Sohn, Development of Green Suspension Ironmaking Technology Based on Hydrogen Reduction of Iron Oxide Concentrate: Rate Measurements, Ironmak. Steelmak. **37**, 81 (2010).

[9] *MIDREX® Process*, https://www.midrex.com/technology/midrex-process/.

[10] *Hybrit*, https://www.hybritdevelopment.se/en/.

[11] S. Mukherjee, S. V. Devaguptapu, A. Sviripa, C. R. F. Lund, and G. Wu, Low-temperature ammonia decomposition catalysts for hydrogen generation, Appl. Catal. B Environ. **226**, 162 (2018).

[12] S. F. Yin, B. Q. Xu, X. P. Zhou, and C. T. Au, A mini-review on ammonia decomposition catalysts for on-site generation of hydrogen for fuel cell applications, Appl. Catal. Gen. **277**, 1 (2004).

[13] E. Morgan, J. Manwell, and J. McGowan, Wind-powered ammonia fuel production for remote islands: A case study, Renew. Energy **72**, 51 (2014).

[14] H. Ishaq, M. F. Shehzad, and C. Crawford, Transient modeling of a green ammonia production system to support sustainable development, Int. J. Hydrog. Energy (2023).

[15] S. Hosokai, Y. Kasiwaya, K. Matsui, N. Okinaka, and T. Akiyama, Ironmaking with Ammonia at Low Temperature, Environ. Sci. Technol. **45**, 821 (2011).

[16] N. Yasuda, Y. Mochizuki, N. Tsubouchi, and T. Akiyama, Reduction and Nitriding Behavior of Hematite with Ammonia, ISIJ Int. **55**, 736 (2015).

[17] I. Iwamoto, A. Kurniawan, H. Hasegawa, Y. Kashiwaya, T. Nomura, and T. Akiyama, Reduction Behaviors and Generated Phases of Iron Ores using Ammonia as Reducing Agent, ISIJ Int. 155 (2022).

[18] Y. Ma, J. W. Bae, S.-H. Kim, M. Jovičević-Klug, K. Li, D. Vogel, D. Ponge, M. Rohwerder, B. Gault, and D. Raabe, Reducing Iron Oxide with Ammonia: A Sustainable Path to Green Steel, Adv. Sci. **10**, 2300111 (2023).

[19] T. Triana, G. A. Brooks, M. A. Rhamdhani, and M. I. Pownceby, Iron Oxide Direct Reduction and Iron Nitride Formation Using Ammonia: Review and Thermodynamic Analysis, J. Sustain. Metall. **10**, 1428 (2024).

[20] M. Jovičević-Klug, Y. Ma, P. Jovičević-Klug, J. M. Prabhakar, M. Rohwerder, and D. Raabe, Thermal Kinetics and Nitriding Effect of Ammonia-Based Direct Reduction of Iron Oxides, ACS Sustain. Chem. Eng. **12**, 9882 (2024).

[21] A. Steinfeld, P. Kuhn, and J. Karni, High-temperature solar thermochemistry: Production of iron and synthesis gas by Fe3O4-reduction with methane, Energy **18**, 239 (1993).

[22] D. Fernández-González, J. Prazuch, Í. Ruiz-Bustinza, C. González-Gasca, J. Piñuela-Noval, and L. Verdeja González, Iron Metallurgy via Concentrated Solar Energy, Metals **8**, 873 (2018).

[23] S. Li, H. Zhang, J. Nie, R. Dewil, J. Baeyens, and Y. Deng, The Direct Reduction of Iron Ore with Hydrogen, Sustainability **13**, 8866 (2021).

[24] S. Abanades and S. Rodat, Solar-aided direct reduction of iron ore with hydrogen targeting carbon-free steel metallurgy, Renew. Energy **235**, 121297 (2024).

[25] B. Sanglard, B. Huneau, J. Carrey, and S. Lachaize, Towards solar iron metallurgy: Complete hydrogen reduction of iron ore pellets under a concentrated light flux, Sol. Energy **284**, 113072 (2024).

[26] O. Levenspiel, *Chemical Reaction Engineering*, 3rd ed. (Wiley, New York Weinheim, 1999).

[27] A. Ranzani Da Costa, La Réduction Du Minerai de Fer Par l'hydrogène : Étude Cinétique, Phénomène de Collage et Modélisation, Insitut National Polytechnique de Laurraine, 2011.

[28] B. Sanglard, Le Solaire à Concentration Comme Brique Élémentaire d'une Société Pérenne ? - Réduction Directe d'oxyde de Fer Par l'hydrogène et l'ammoniac et Analyse de Cycle de Vie d'une Parabole Solaire Pour La Transformation Alimentaire., Thèse, Institut National des Sciences Appliquées, 2023.

[29] B. Sanglard, S. Lachaize, J. Carrey, and L. Tiruta-Barna, Life cycle assessment of a parabolic solar cooker and comparison with conventional cooking appliances, Sustain. Prod. Consum. **42**, 211 (2023).

[30] *World Steel in Figures 2023*, https://worldsteel.org/data/world-steel-in-figures-2023/.

[31] M. Gorgolewski, The implications of reuse and recycling for the design of steel buildings, Can. J. Civ. Eng. **33**, 489 (2006).

[32] M. Pongiglione and C. Calderini, Material savings through structural steel reuse: A case study in Genoa, Resour. Conserv. Recycl. **86**, 87 (2014).

[33] J. Johnson, B. K. Reck, T. Wang, and T. E. Graedel, The energy benefit of stainless steel recycling, Energy Policy **36**, 181 (2008).

[34] N. T. Nguyen, T.-T. Bui, and Q.-B. Bui, Fiber reinforced concrete for slabs without steel rebar reinforcement: Assessing the feasibility for 3D-printed individual houses, Case Stud. Constr. Mater. **16**, e00950 (2022).

[35] E. M. Palmeira, G. L. S. Araújo, and E. C. G. Santos, Sustainable Solutions with Geosynthetics and Alternative Construction Materials—A Review, Sustainability **13**, 12756 (2021).

[36] J. Josiah Marut, J. O. Alaezi, and I. C. Obeka, A Review of Alternative Building Materials for Sustainable Construction Towards Sustainable Development, J. Mod. Mater. **7**, 68 (2020).

[37] A. Lundström, B. Andersson, and L. Olsson, Urea thermolysis studied under flow reactor conditions using DSC and FT-IR, Chem. Eng. J. **150**, 544 (2009).

[38] D. Wang, S. Hui, and C. Liu, Mass loss and evolved gas analysis in thermal decomposition of solid urea, Fuel **207**, 268 (2017).